ELSEVIER

Journal of Fluids and Structures 20 (2005) 577–587

JOURNAL OF FLUIDS AND STRUCTURES

www.elsevier.com/locate/jfs

Analysing fluid loadings on moving bluff bodies using proper orthogonal decomposition

X. Amandolèse[a], C. Crémona[b,*]

[a]*Institut Aérotechnique, Saint-Cyr l'Ecole, France*
[b]*Laboratoire Central des Ponts et Chaussées, Paris, France*

Received 24 August 2004; accepted 22 February 2005
Available online 10 May 2005

Abstract

Numerical simulations and experimental measurements of the fluid loadings on three typical fixed or moving bluff bodies are presented and analysed. The numerical approach is based on an efficient finite-element solver using an Arbitrary Lagrangian–Eulerian formulation for solving the two-dimensional incompressible Navier–Stokes equations with moving domains. Experimental tests consist of unsteady pressure measurements performed during sectional model tests. The Proper Orthogonal Decomposition applied to the wall pressure distributions is used in addition to spectral analyses in order to explain complex flow signature and motion-induced mechanisms. Effects of body shapes and dynamic characteristics (reduced wind speed, motion amplitude) on flow response and resulting loads are then examined.

Keywords: Bridge aerodynamics; Proper orthogonal decomposition; CFD; Motion-induced vibrations

1. Introduction

Since the spectacular failure of the Tacoma Narrows bridge in 1940, bridge deck aerodynamics and aeroelasticity have received a large amount of attention. Methodologies for wind tunnel tests were first proposed by Farquharson (1949–1954), along with early work on aeroelastic stability carried out by Bleich (1948). Then the flutter instability problem which was first investigated experimentally and theoretically in aeronautics by Wagner (Theodorsen, 1935), was extended by Bisplinghoff and Ashley (1962) and Scanlan and Tomko (1971), Sabzevari and Scanlan (1969) and analytical formulations of forces acting on vibrating elongated bluff-bodies like long-span bridge decks were proposed [see Scanlan (1993) for a review].

Several experimental approaches are used to assess the response of bridge decks to wind excitation: sectional tests, taut-strip tests, full-bridge tests and full-scale measurements. Amongst all these approaches, the sectional tests remain widely used in the design phase of bridges. The sectional model approach is based on structural dynamic analysis coupled with analytical wind force models (Scanlan and Tomko, 1971; Scanlan 1993, 1997), introducing steady and unsteady coefficients which have to be identified through specific model tests in wind tunnels. In this approach, the two-dimensionality of the flow is mainly assumed but can be corrected with the aim of spanwise coherent function (Scanlan

*Corresponding author. Tel.: +33 1 4043 5344; fax: +33 1 4043 6515.
E-mail address: christian.cremona@lcpc.fr (C. Crémona).

0889-9746/$ - see front matter
doi:10.1016/j.jfluidstructs.2005.02.008

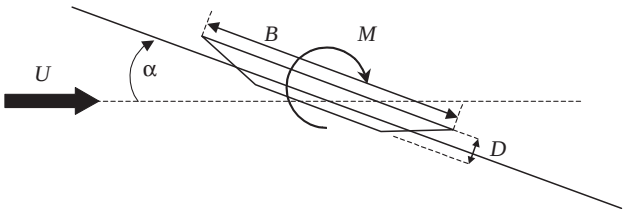

Fig. 1. Cross-section displacement and pitching moment convention.

et al., 1997). These wind force models, and more specifically the aeroelastic ones which account for the motion-dependant response through the so-called aerodynamic damping and stiffness, involve motion-induced fluid mechanisms that are still under investigation (Matsumoto, 1997). Moreover, progress in Computational Fluid Dynamics and computer technologies provides today an alternative way for flutter derivative identification and research on involved fluid mechanisms (Tamura and Itoh, 1993). Indeed, bridge decks, unless they are well streamlined, generate complex flow signatures due to sharp-edge flow separation and flow instabilities (impinging shear layer instabilities, trailing-edge vortex shedding) leading to particular unsteady aerodynamic pressure fields. Any change of the boundary conditions due to the deck vibration induces flow adaptation involving complex motion-induced fluid mechanisms which depend on the deck shape and on the vibrational characteristics according to the mean cross flow speed.

Within this context, the present paper is focused on the study of two-dimensional fluid mechanisms and resulting loads on three typical bluff bodies: two rectangular shapes with side-ratios of 4 and 8, and the deck section of the Millau bridge project. These shapes are moving in forced harmonic pitching motion in a transverse flow. In order to apprehend basic flow phenomena the present study is also restricted to laminar flows. For this reason, the attention is restricted to the study of the unsteady pressure fields and resulting forces.

Both numerical simulations obtained from moving-grid computation of the Navier–Stokes equations, based on an efficient finite-element solver using an Arbitrary Lagrangian Eulerian (ALE) formulation, and dynamic sectional model tests in wind tunnels have been performed and analysed. The Proper Orthogonal Decomposition (POD) applied to the surface pressure distributions is used in addition to spectral analyses in order to explain motion-induced mechanisms, and to understand their influence on loads and aeroelastic reduced-order models. Effects of body shapes and dynamic characteristics on resulting loads are then examined. This paper concludes by highlighting the conditions for using a CFD solver for the study of large-scale flow behaviour around moving bluff bodies. In the present paper incidence angle and pitching moment are defined as in Fig. 1. The pitching motion amplitude is denoted $\tilde{\alpha}$ and the reduced velocity is defined as $U^* = U/fB$, where U is the mean cross-flow velocity, B is the chord of the sectional model and f the frequency of the imposed pitching motion $\alpha(t) = \tilde{\alpha}\sin(2\pi ft)$.

2. Methods of investigation

2.1. Experimental tools

Experimental tests were carried out in the atmospheric wind tunnel of the CSTB centre in Nantes (France) using an experimental rig (Cremona et al., 2003). A sectional model is able to oscillate in pitch with controlled frequency and amplitude. Tested models are two rectangular shapes with side-ratios of 4 and 8, and a representative two-dimensional cross-section of the Millau bridge project. Unsteady 2-D pressure fields were measured with approximately 60 pressure taps installed on the surface of each model (Figs. 2–4).

The flow condition was mainly smooth with an approximate turbulence intensity of 0.7%. The Reynolds number was close to 2.8×10^5 for rectangular cylinders and 6.4×10^5 for the Millau section.

2.2. Numerical tools

In order to numerically assess fluid loading responses on moving bodies, the unsteady incompressible Navier–Stokes equations have to be solved within a moving domain. A finite-element solver developed at the INRIA research institute in Rocquencourt by F. Hecht and C. Pares-Madronal (Pares–Madronal, 1992) has been used. The approach is based on a purely Eulerian approach, modified to deal with an Arbitrary Lagrangian–Eulerian (ALE) formulation. A brief

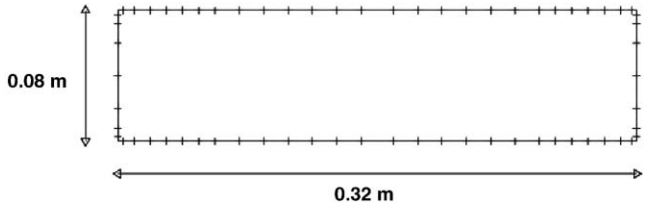

Fig. 2. Model of the rectangular section with side-ratio 4.

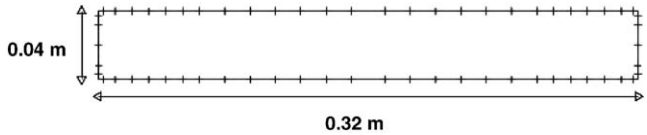

Fig. 3. Model of the rectangular section with side-ratio 8.

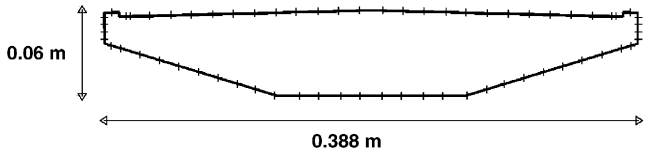

Fig. 4. Model of the "Millau" section.

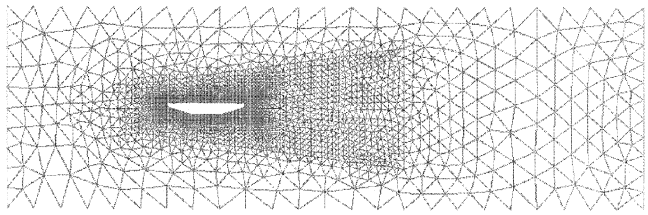

Fig. 5. Typical mesh for the "Millau bridge section" numerical simulations.

overview of this particular approach is presented here. The main characteristics of the algorithm are described in Piperno (1997).

The space-discretization of the original solver is based on a classical finite element formulation. The computational area is an unstructured triangulation of the domain, verifying classical regularity conditions. The time-discretization is based upon a first-order characteristics method. Computation of upwind characteristics is based on a first-order time-approximation. When the body moves, the fluid area is deformed. The triangulation is then modified at each time step. In the ALE formulation each element of the triangulation is allowed to move using an elastic analogy. A compatible velocity field in moving coordinates must then be specified to compute a generalized Stokes problem at each time step.

The fluid domain is a rectangular domain with dimension $11B \times 14D$, where B is the chord length and D the depth related to the body sizes. Since no turbulence models have been introduced in the numerical approach, the scales of the simulated phenomena depend strongly on the Reynolds number, mesh refinement choice and associated time step. Influence of these numerical parameters have been performed by Amandolèse et al. (2000) in order to find reasonable choices in relation to the large scales of fluid mechanisms that dominate the steady and the aeroelastic responses. Results reported in this paper concern calculations performed for moderate Reynolds numbers, roughly ten times smaller than the wind tunnel conditions ($\mathrm{Re} = 2 \times 10^4$ for R4 and R8; $\mathrm{Re} = 5 \times 10^4$ for Millau) with relatively rough space and time discretizations (Fig. 5 and Table 1).

Table 1
Numerical simulations characteristics

Section	Total number of nodes	Number of surface nodes	δh	$\delta h/\delta T$
R4, R8	≈ 5000	300	0.008	2
Millau	≈ 5500	390	0.006	3

In the table, $\delta h = \Delta h/B$ and $\delta T = \Delta T U/B$ are the relative element dimension in the vicinity of the body surface and the nondimensioned time step, respectively. Even if, as emphasized further, some discrepancies can be noticed with the experiments, especially for the prediction of the mean local flow reattachment, numerical parameters that have already been chosen permit us to understand fluid mechanisms and the corresponding unsteady pressure evolution when bodies oscillate.

2.3. The Proper Orthogonal Decomposition

The Proper Orthogonal Decomposition (POD) is a particularly well-suited technique for the analysis of unsteady fluid components and for the detection of coherent structures (Holmes et al., 1996). It is mainly used for the identification of reduced order models of the Navier–Stokes equations. This technique also seems to be powerful for studying fluid loading on fixed and moving bluff-bodies (Hémon and Santi, 2002) and offers the advantage of capturing the physics simultaneously in space and time. In this special case, the method consists on the decomposition of the nondimensioned wall pressure field $\{C_p(t)\}$ on proper orthogonal functions which are normalized eigenvectors of the two-point correlation matrix $[R_c]$ of the unsteady wall pressure distribution around the body:

$$\{C_p(t)\} = \sum_{k=1}^{k=m} \mu_k(t)\{W_k\}, \tag{1}$$

where m is the number of pressure taps used for the analysis, $(W_k)_{k=1,m}$ is the series of the m normalised orthogonal eigenvectors which are associated with the decreasing series $(\lambda_k)_{k=1,m}$ of the eigenvalues of the matrix $[R_c]$:

$$\begin{aligned} &[R_c]\{W_k\} = \lambda_k\{W_k\}, \\ &{}^t\{W_k\}\{W_j\} = \delta_{k,j}, \end{aligned} \tag{2}$$

and $[R_c]$ is defined as

$$\begin{aligned} &[R_c] = [r_c(i,j)]_{i=1,m,j=1,m}, \\ &r_c(i,j) = \frac{1}{N}\sum_{p=1}^{N} C_{p,i}(t_p)C_{p,j}(t_p). \end{aligned} \tag{3}$$

Then the principal components μ_k are given by projecting the pressure field onto the kth proper function:

$$\mu_k(t) = {}^t\{W_k\}\{C_p(t)\}. \tag{4}$$

The main interest of this method is that the set of proper functions for the decomposition is inherent to the mechanisms involved around the body; indeed, the proper functions are not *a priori* chosen but depend on the spatial pressure correlation around the body. Furthermore, as reported in Hémon and Santi (2002), because of the orthogonality of the normalized set of proper functions, each eigenvalue λ_k is equal to the mean quadratic value of the principal component μ_k:

$$\lambda_k = \overline{[\mu_k(t)]^2} \tag{5}$$

and are representative of the energy level contribution of each proper function in the average of the mean quadratic pressure distribution along the body:

$$\frac{1}{m}\sum_{k=1}^{k=m}\overline{[C_{P,k}(t)]^2} = \sum_{k=1}^{k=m}\lambda_k. \tag{6}$$

3. Preliminary POD analysis

In order to illustrate the efficiency of the POD technique for the analysis of pressure loads due to motion-induced fluid mechanisms, numerical simulation of a rectangular section with side-ratio 8 in pitching motion ($\tilde{\alpha} = 0.066$ rad; $U^* = 6$) are presented in this section. The moment coefficient response is reported in Fig. 6 along with its associated power spectrum. As expected, the time-domain signal exhibits a dominating harmonic component at a reduced frequency close to $1/U^*$. Small contributions of the first and second harmonic components also appear as highlighted in the POD analysis. POD analysis has been applied to the calculated unsteady wall pressure distribution.

The decreasing series $(\lambda_k)_{k=1,m}$ of the eigenvalues of the two-point correlation matrix $[R_c]$ is presented in Fig. 7.

Because the POD decomposition has been performed on the total pressure distribution without excluding the mean value, the first proper function is representative of the mean pressure distribution. In Fig. 8, the mean pressure

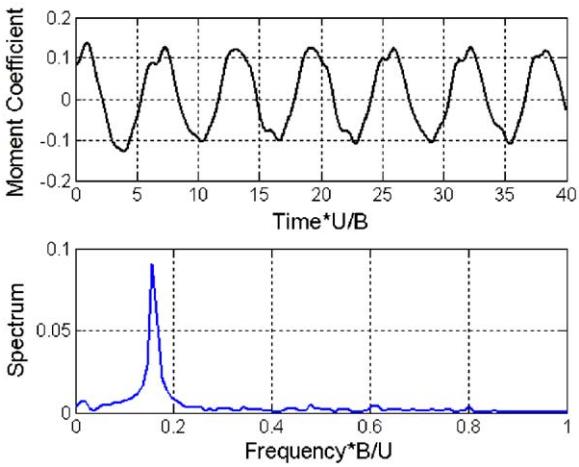

Fig. 6. Response and power spectrum of pitching moment (R8 section).

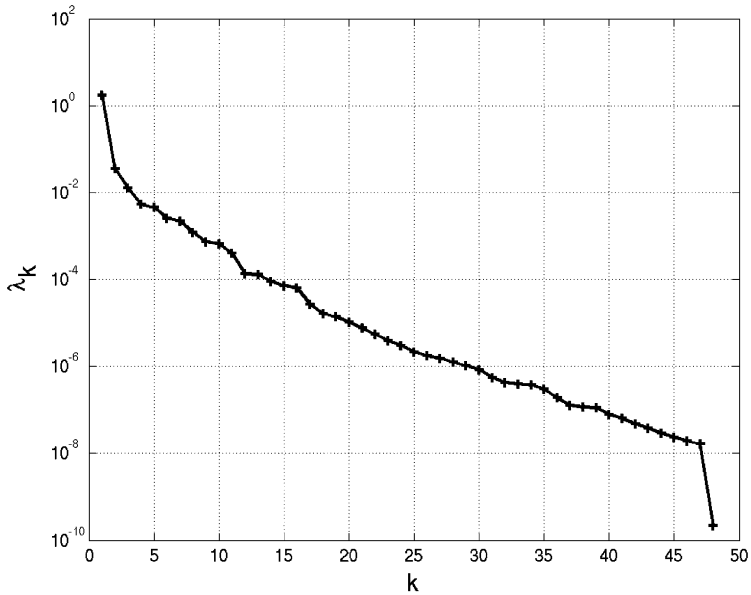

Fig. 7. Eigenvalues of the correlation matrix $[R_c]$.

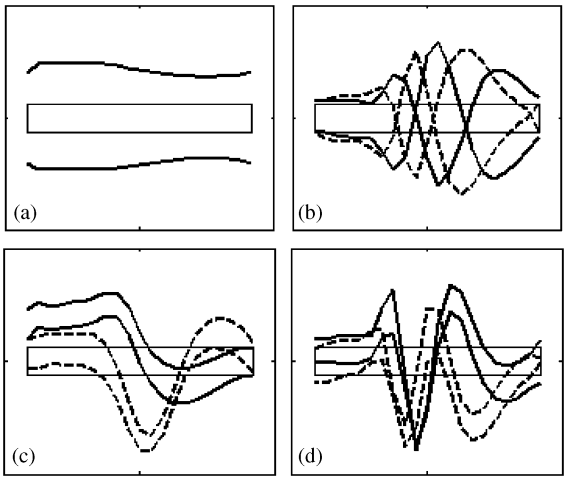

Fig. 8. Mean pressure distribution and 6 first unsteady proper functions (intrados and extrados). (a) Mean pressure; (b) W2 and W3; (c) W4 and W5; (d) W6 and W7.

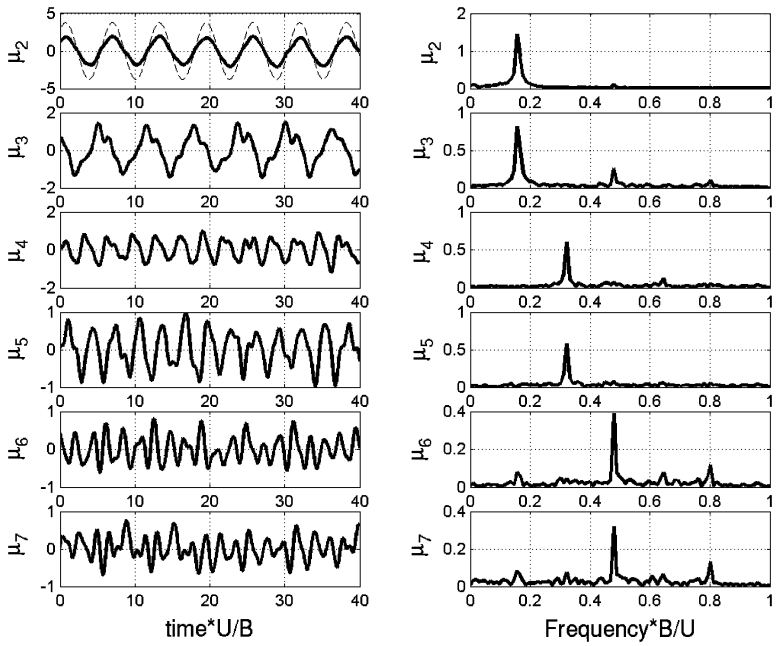

Fig. 9. Responses and spectrum of the first six unsteady principal components.

distribution (for intrados and extrados) is reported with the six first proper functions which are representative of the unsteady pressure loading. Time-domain response and power spectrum of their associated principal components are reported in Fig. 9. The contribution of each proper function $\{W_k\}$ to the moment response has been calculated by integrating the associated pressure contribution:

$$\{C_P^k(t)\} = \mu_k(t)\{W_k\}. \tag{7}$$

The sum of the first two, first four and first six unsteady proper functions to the moment coefficient are reported in Fig. 9.

These results show that the unsteady characteristics of the moment coefficient are mainly represented by using the first six unsteady proper functions (the first proper function being denoted as the "mean" proper function). According

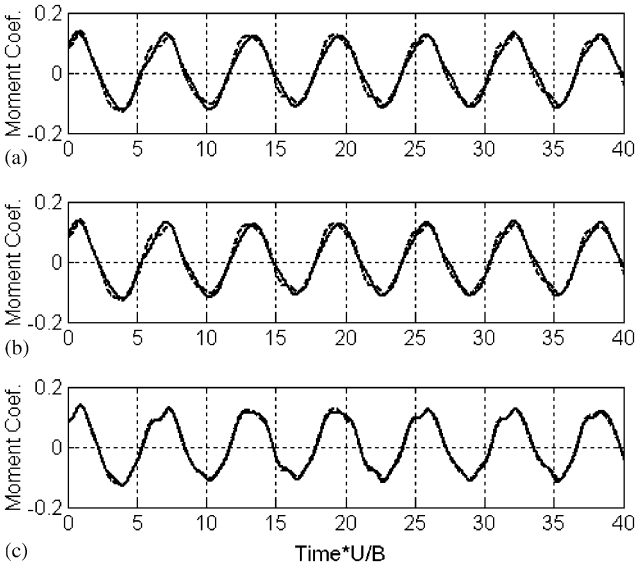

Fig. 10. Contribution of the first six unsteady proper functions to the moment coefficient response; - - -, total response. (a) First two unsteady functions; (b) first four unsteady functions; (c) first six unsteady functions.

to their associated principal component characteristics (Fig. 9) proper functions 2 and 3 are representative of the pressure response at the imposed reduced frequency while proper functions 4 and 5 and proper functions 6 and 7 are representative of the pressure response at the first and second harmonic of the imposed frequency, respectively. In Fig. 10 the pitching motion response (in degrees, dashed curve) is compared to the principal component response associated to the second proper function. This figure shows that $\mu_2(t)$ is nearly in phase with $\alpha(t)$, while a transfer function between $\mu_3(t)$ and $\mu_2(t)$ reveals that these two principal components are in quadrature at the pitching motion frequency; $\mu_3(t)$ is therefore nearly in phase with $\dot{\alpha}(t)$.

The contribution of each proper function to the in phase and quadrature response of the resulting moment has been calculated with reference to the linear aeroelastic model of the pitching moment in the Scanlan notation (Scanlan, 1993):

$$\tilde{C}_M^{ae}(t) = 2\left[KA_2^*(K)\frac{B\dot{\alpha}(t)}{U} + K^2A_3^*(K)\alpha(t)\right], \tag{8}$$

where A_3^*, A_2^* are the stiffness and damping flutter derivatives, respectively. The results show that the cumulative contribution due to proper functions 2 and 3 predicts the linear aeroelastic response of the moment coefficient with an r.m.s. error of 3%. Proper function 2 is, respectively, responsible for 95% of the stiffness flutter derivative A_3^*, while proper function 3 contributes to more than 90% of the damping coefficient A_2^*. Stiffness and damping behavior of the two first unsteady proper functions have been observed for various configurations.

4. Aeroelastic results for bluff sections oscillating in pitch

Numerical simulations obtained from moving-grid computations of the Navier–Stokes equations have been performed on the rectangular sections and on the Millau section for various dynamic configurations. In order to assess the capability of the numerical approach to capture the fluid loading responses to pitching motions, comparisons between numerical results and experiments are performed for reduced velocity $U^* = 6$, $\tilde{\alpha} = 0.07$ rad for the R4 rectangular section (Figs. 11 and 12) and for the Millau cross-section (Figs. 13 and 14). Mean pressure distribution on the upper surface and aeroelastic proper functions (i.e. stiffness proper function W_2 and damping proper function W_3 according to the POD projection) are shown. In Figs. 13 and 14 the proper functions are multiplied by the standard deviation of the related principal component in order to take into account the fluctuation amplitude.

The R4 results show that, despite an underestimation of the pressure level all along the upper surface, the mean pressure distribution is correctly evaluated with a good prediction of the length of the mean separated region. The

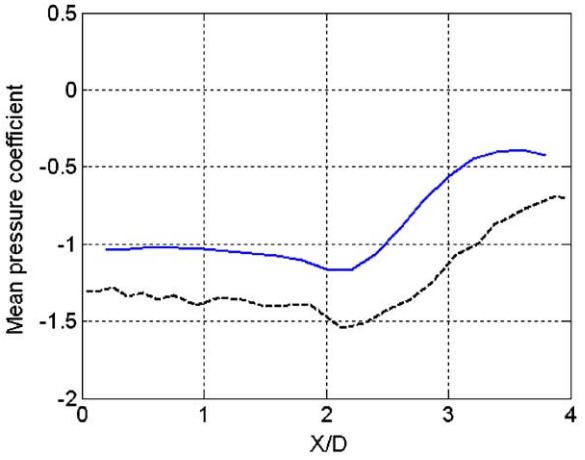

Fig. 11. Mean pressure distribution on the R4 upper surface: - - -, experimental; —, numerical.

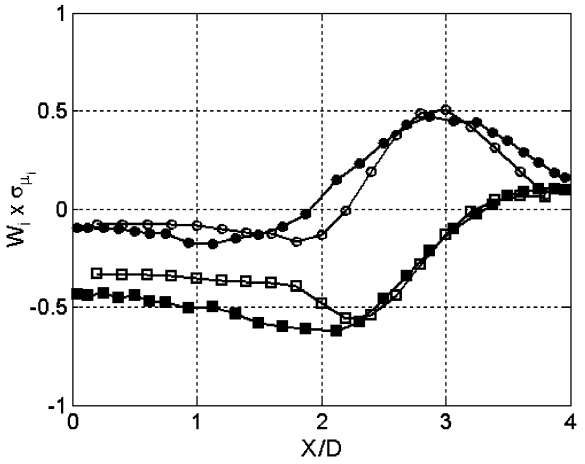

Fig. 12. Aeroelastic pressure distribution on the R4 upper surface: ■, proper function W2 (experimental); □, proper function W2 (numerical); ●, proper function W3 (experimental); ○, proper function W3 (numerical).

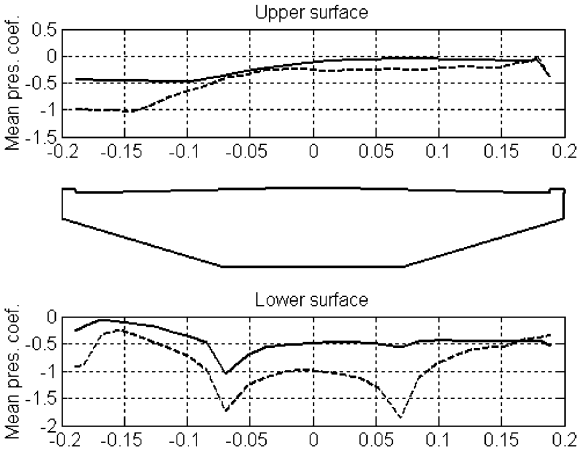

Fig. 13. Mean pressure distribution around the Millau section: - - -, experimental; —, numerical.

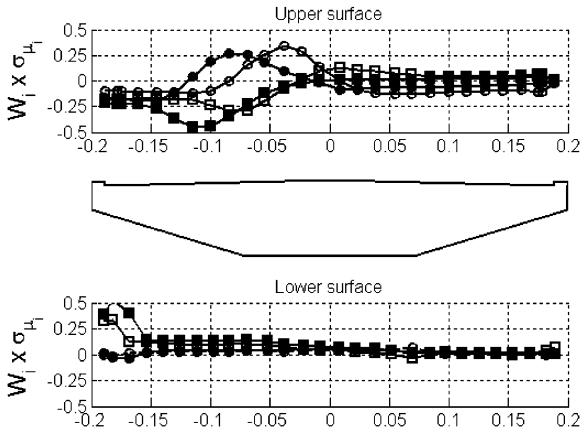

Fig. 14. Aeroelastic pressure distribution around the Millau section: ■, proper function W2 (experimental); □, proper function W2 (numerical); ●, proper function W3 (experimental); ○, proper function W3 (numerical).

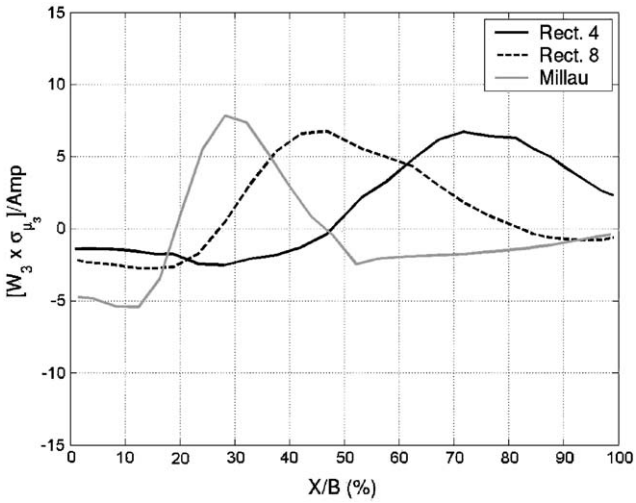

Fig. 15. Body shape influence on the "damping" pressure distribution (upper surface).

numerical prediction of the proper functions 2 and 3 are also close to experiments highlighting that the motion-induced fluid mechanisms are well predicted.

For the Millau section, aeroelastic proper functions reported in Fig. 13 show that the fluid loading response is mainly due to leading edge separated shear layer adaptation to pitching motion on both the upper surface and the lower surface. As a consequence, the significant discrepancy noticed on the prediction of the mean pressure distribution over the elastic center ($X>0$) does not influence the aeroelastic prediction. Nevertheless one can notice that the length of the mean leading edge separated region on the upper surface is numerically overestimated. As a consequence, the shapes of proper functions 2 and 3 are close to experiments but shifted toward the elastic center (located at the middle of the chord). This could generate a significant underestimation of the absolute values of A_3^*, A_2^* which are positive and negative for such a streamlined section, respectively.

Body shape influence on aeroelastic pressure responses is highlighted in Fig. 15. The damping proper function 3, extracted from POD analyses of unsteady pressure measurements, is presented for the R4, R8 and Millau sections ($\tilde{\alpha}=0.07$ rad; $U^*=6$). As reported previously, the relative position of the fluid adaptation domain depends on the length of the mean leading edge separated region. The damping proper function 3 for the R4 section is important and positive for $X/B>0$ which indicates that the pressure distribution work per pitching cycle is positive, i.e. the A_2^* flutter derivative is positive. For higher side-ratios, the length of the mean leading edge separated region decreases. Because

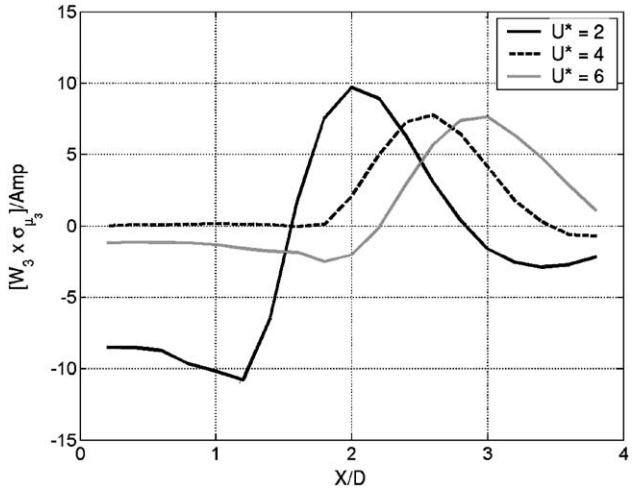

Fig. 16. Influence of the reduced velocity on the "damping" pressure distribution (R4 upper surface).

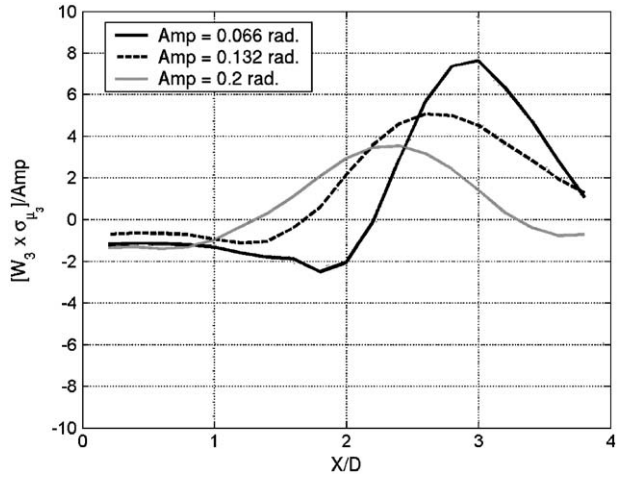

Fig. 17. Influence of the pitching amplitude on the "damping" pressure distribution (R4 upper surface).

there is no motion-induced vortex generated along the surface that could change the damping proper function shape, A_2^* decreases for the R8 section and is negative for the Millau section.

Influence of the reduced velocity and pitching motion amplitude on the damping proper functions for the R4 section is reported in Figs. 16 and 17. Those results are issued from the POD analysis of numerical simulations. The shape of the damping pressure distribution for $U^* = 4$ is close to the one reported for $U^* = 6$, but the position of the fluid adaptation domain moves towards the elastic center, and then A_2^* will decrease. For $U^* = 2$ the damping proper function changes due to a stronger shear imposed on the leading-edge separated region. The sign of the associated A_2^* flutter derivative then changes and becomes negative. As highlighted in Fig. 17, the pitching motion amplitude has a significant influence on the aeroelastic pressure response. Indeed it tends to shift the fluid adaptation domain towards the elastic center when the amplitude is decreasing. Consequently, the A_2^* flutter derivative is reduced.

5. Conclusions

Pressure responses around two rectangular sections and a deck section of the Millau bridge project in pitching motion have been studied using the Proper Orthogonal Decomposition. Results have shown that this technique is a simple and

powerful tool that highlights the influence of the body shapes and motion characteristics (reduced velocity, amplitude) on the aeroelastic pressure responses and resulting flutter derivatives. Indeed, two unsteady proper functions seem to be sufficient to mimic satisfactorily linear aeroelastic responses. Results have also shown that aeroelastic pressure responses are mainly due to the adaptation of the leading edge separated region. The validation of the separated region is a prerequisite for performing accurate numerical aeroelastic predictions. It is particularly important for streamlined sections for which the predictions of the local flow separation and reattachment are not so easy to handle.

Acknowledgments

CSTB and INRIA (France) are gratefully acknowledged for their experimental and computational support.

References

Amandolèse, X., Bourquin., F., Cremona, C., 2000. Numerical investigation of aerodynamic forces on rectangular cylinders and generic bridge deck sections. In: Ziada, S., Staubli, T. (Eds.), Flow Induced Vibration. Balkema, Dordrecht, pp. 141–148.

Bisplinghoff, R.L., Ashley, H., 1962. Principles of Aeroelasticity. Wiley, New York.

Bleich, F., 1948. Dynamic instability of truss-stiffened suspension bridges under wind action. Proceedings ASCE 74, 1269–1314.

Cremona, C., Amandolese, X., Grillaud, G., Flamand, O., 2003. Fluid-loading simulations around bridge decks. Revue Francaise de Genie Civil 7 (6), 717–743.

Farquharson, F.B., 1949–1954. Aerodynamic stability of suspension bridges. University of Washington. Bulletin 16, Parts 1–4.

Hémon, P., Santi, F., 2002. On the aeroelastic behavior of rectangular cylinders in cross-flow. Journal of Fluids and Structures 16, 855–889.

Holmes, P., Lumley, J.L., Berkooz, G., 1996. Turbulence, Coherent Structure and Symmetry. Cambridge University Press, Cambridge.

Matsumoto, M., 1997. Torsional flutter of bluff bodies. Journal of Wind Engineering and Industrial Aerodynamics 69–71, 871–882.

Pares-Madronal, C., 1992. Etude mathématique et approximation numérique de quelques problèmes aux limites de la mécanique des fluides. Ph. D. Thesis (in French), University of Paris, France.

Piperno, S., 1997. Explicit/implicit fluid-structure staggered procedures with a structural predictor and fluid subcycling for 2d inviscid aeroelastic simulations. International Journal for Numerical Methods in Fluids 25, 1207–1226.

Sabzevari, A.M., Scanlan, R.H., 1969. Aerodynamic investigation of box girder bridges. ASCE Journal of the Structural Division 95, 1517–1532.

Scanlan, R.H., 1993. Problematics in formulation of wind-force models for bridge decks. ASCE Journal of Engineering Mechanics 119, 1353–1375.

Scanlan, R.H., 1997. Amplitude and turbulence effects on bridge flutter derivatives. ASCE Journal of Structural Engineering 123, 232–236.

Scanlan, R.H., Tomko, J.J., 1971. Airfoil and bridge flutter derivatives. ASCE Journal of Engineering Mechanics 109, 586–603.

Scanlan, R.H., Jones, N.P., Lorendeaux, O., 1997. Comparison of taut-srtip and section-model-based approaches in long-span bridge aerodynamics. Journal of Wind Engineering and Industrial Aerodynamics 72, 275–287.

Tamura, T., Itoh, Y., 1993. Numerical investigation on the aeroelastic instability of bluff cylinders. Journal of Wind Engineering and Industrial Aerodynamics 46–47, 557–566.

Theodorsen, T., 1935. General theory of aerodynamic instability and the mechanism of flutter. NACA Report No. 496, USA.